THE JOURNAL OF PHYSICAL CHEMISTRY Letters

pubs.acs.org/JPCL Letter

Compact Bases for Vibronic Coupling in Spectral Simulations: The Photoelectron Spectrum of Cyclopentoxide in the Full 39 Internal Modes

Yifan Shen* and David R. Yarkony*

Cite This: J. Phys. Chem. Lett. 2020, 11, 7245−7252 Read Online

ACCESS | Metrics & More | Article Recommendations

ABSTRACT: We report an algorithm to automatically generate compact multimode vibrational bases for the Köppel−Domcke−Cederbaum (KDC) vibronic coupling wave function used in spectral simulations of moderate-sized molecules. As a full quantum method, the size of the vibronic expansion grows exponentially with respect to the number of vibrational modes, necessitating compact bases for moderate-sized systems. The problem of generating such a basis consists of two parts: one is the choice of vibrational normal modes, and the other is the number of phonons allowed in each mode. A previously developed final-state-biased technique addresses the former part, and this work focuses on the latter part: proposing an algorithm for generating an optimal phonon distribution. By virtue of this phonon distribution, compact and affordable bases can be automatically generated for systems with on the order of 15 atoms. Our algorithm is applied to determine the nonadiabatic photoelectron spectrum of cyclopentoxide in the full 39 internal modes.

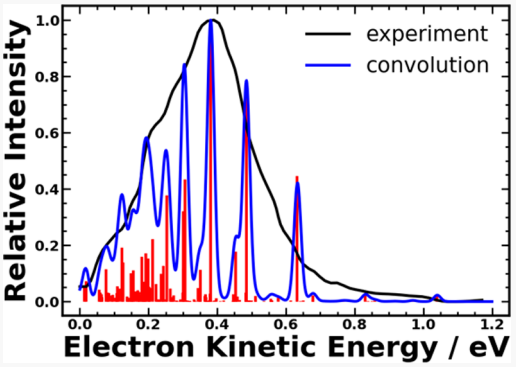

The Köppel−Domcke−Cederbaum (KDC) vibronic coupling method[1−4] is an often-employed approach[5−16] for determining nonadiabatic spectral intensities, producing discrete line spectra. In its time-independent form, the KDC algorithm uses a Lanczos procedure to diagonalize the molecular Hamiltonian in a direct product basis of harmonic nuclear vibrations and diabatic electronic states. A recently reported fine-grained parallel Lanczos solver[17] is able to handle billions of basis functions (if the eigenvectors are not demanded). However, the size of the vibronic coupling expansion grows exponentially with respect to the number of vibrational modes, limiting its application to small molecules in the absence of compact vibrational bases. Compact vibrational bases are also demanded in variational methods for computing vibrational levels.[18−21]

To determine a vibrational basis, normal modes and the number of phonons allowed in each mode are required. In typical cases, the spectral transition from a simple initial state produces complicated final states, which are vibronically coupled levels whose electronic states can be coupled by conical intersections.[22−25] Some improvements have been made to partially tackle the problem. A generating function technique[26] has eliminated the "Franck−Condon region as origin" constraint, allowing final-state-biased normal modes to be utilized.[26−33] However, the phonon distribution has long been left to chemical intuition plus trial and error, which is overwhelmed in the moderate-dimensional case by its myriad of possibilities.

Aiming at the second piece of the puzzle, in this work we propose an algorithm for generating an optimal phonon distribution of the final-state-biased normal modes. The algorithm provides a one parameter mapping $\mathbf{N}(M)$ where N_j is the maximum number of phonons permitted in the jth mode. M is described in eq 10, where it is used to optimize the total overlap between the initial vibronic state and the final-state-biased basis. The comparatively small magnitude of $\mathbf{N}$ permits the Lanczos routine used to diagonalize the vibronic Hamiltonian (eq 6) to employ explicitly orthogonalized Krylov vectors.

In order to explain the construction of the vibronic basis we begin with a brief review of the KDC approximation. The initial vibronic state is given by

$$\Psi_J^{\text{init}}(\mathbf{r}, \mathbf{Q}) = \phi^J(\mathbf{Q})\, \psi^{\text{init}}(\mathbf{r}; \mathbf{Q}) \tag{1}$$

Received: July 18, 2020
Accepted: August 10, 2020
Published: August 10, 2020

https://dx.doi.org/10.1021/acs.jpclett.0c02199
J. Phys. Chem. Lett. 2020, 11, 7245−7252

where $\mathbf{r}$ denotes the electronic coordinates, $\mathbf{Q}$ is a set of nuclear mass-weighted normal coordinates to be defined below, ϕ^J is the nuclear wave function (usually the ground vibrational level, $J = 0$, of the initial electronic state), and ψ^{init} is the adiabatic electronic wave function. The final vibronic state is expanded as

$$\Psi_K^{\text{final}}(\mathbf{r}, \mathbf{Q}) = \sum_{i=1}^{N^{\text{state}}} \phi_i^K(\mathbf{Q})\, \psi_i^d(\mathbf{r}; \mathbf{Q}) \tag{2}$$

where N^{state} is the number of ψ_i^d, the quasidiabatic[34,35] electronic states. In photoelectron spectroscopy ψ_i^d has a continuum electron,[36−39] which is suppressed. ϕ_i^K, the vibrational function associated with ψ_i^d, is in turn expanded in a multimode vibrational basis

$$\begin{aligned}\phi_i^K(\mathbf{Q}) &= \sum_{\mathbf{n}=0}^{\mathbf{N}} D_{\mathbf{n}}^{K,i} |\mathbf{n}(\mathbf{Q})\rangle \\ &= \sum_{n=1}^{N^{\text{vib}}} D_n^{K,i} \prod_{j=1}^{N^{\text{mode}}} |n_j(Q_j)\rangle, \quad 0 \le n_j < N_j\end{aligned} \tag{3}$$

where $|n_j(Q_j)\rangle$ denotes the n_jth harmonic oscillator function for mode j, N_j is the maximum number of phonons allowed in the jth mode (the phonon distribution), and N^{vib} is the size of the vibrational basis

$$N^{\text{vib}}(\mathbf{N}) = \prod_{i=1}^{N^{\text{mode}}} N_i \tag{4}$$

N^{mode} is the number of vibrational modes (the dimension of $\mathbf{Q}$). In the first sum in eq 3 the vibrational basis is indexed by N^{mode} long vectors $\mathbf{n}$; in the second sum $\mathbf{n}$ has been mapped onto scalars n for notational simplicity. In this vibronic basis, the total molecular Hamiltonian $\mathbf{H}$ is an $N^{\text{vib}}N^{\text{state}} \times N^{\text{vib}}N^{\text{state}}$ real symmetric matrix given by

$$\begin{aligned}H_{ij}^{\mathbf{mn}} &= \langle \mathbf{m}(\mathbf{Q})\, \psi_i^d(\mathbf{r}; \mathbf{Q}) | \hat{H} | \mathbf{n}(\mathbf{Q})\, \psi_j^d(\mathbf{r}; \mathbf{Q}) \rangle \\ &= \langle \mathbf{m}(\mathbf{Q}) | \hat{T}\delta_{ij} + H_{ij}^d(\mathbf{Q}) | \mathbf{n}(\mathbf{Q}) \rangle\end{aligned} \tag{5}$$

where $\hat{T}$ is the nuclear kinetic energy operator, $\mathbf{H}^d$ is the quasidiabatic electronic Hamiltonian. $D_n^{K,i}$ is determined from the nuclear Schrödinger equation

$$\mathbf{H}\mathbf{D}^K = E_K \mathbf{D}^K \tag{6}$$

The spectral amplitude is given by

$$\begin{aligned}A_{JK} &= \langle \Psi_J^{\text{init}}(\mathbf{r}, \mathbf{Q}) | \hat{\mu} | \Psi_K^{\text{final}}(\mathbf{r}, \mathbf{Q}) \rangle \\ &= \sum_{i=1}^{N^{\text{state}}} \sum_{m,n=1}^{N^{\text{vib}}} d_m^J \mu_i^{mn} D_n^{K,i} = \mathbf{d}^J \boldsymbol{\mu} \mathbf{D}^K\end{aligned} \tag{7}$$

where $\hat{\mu}$ is the transition dipole operator, $\phi^J(\mathbf{Q})$ has been expanded in the $|\mathbf{m}(\mathbf{Q})\rangle$ basis, giving $d_m^J = \langle \mathbf{m}(\mathbf{Q}) | \phi^J(\mathbf{Q}) \rangle$ and $\mu_i^{\mathbf{mn}} = \langle \mathbf{m}(\mathbf{Q}) \psi^{\text{init}}(\mathbf{r}; \mathbf{Q}) | \hat{\mu} | \psi_i^d(\mathbf{r}; \mathbf{Q})\, \mathbf{n}(\mathbf{Q}) \rangle$. $\mu_i^{\mathbf{mn}}$, which is usually approximated[1] in photoelectron spectroscopy, can be calculated provided that the basic electronic structure data $\langle \psi^{\text{init}}(\mathbf{r}; \mathbf{Q}) | \hat{\mu} | \psi_i^d(\mathbf{r}; \mathbf{Q}) \rangle_{\mathbf{r}}$ are known.

Equation 6 can be solved using a Lanczos algorithm with $\mathbf{d}^J\boldsymbol{\mu}$ as the seed vector.[4] In this case from eq 7, A_{JK} emerges from the seed vector's contribution to $\mathbf{D}^K$. Note that the complexity of a single Lanczos iteration is $O([N^{\text{vib}}N^{\text{state}}]^2)$, and the limit of our implementation[17] is $N^{\text{vib}}N^{\text{state}} < 10^9$. However, by the nature of the direct product, N^{vib} grows exponentially over N^{mode} (see eq 4). Diagonalization of eq 6 by a Lanczos routine is known to be unstable, but still useful, when N^{vib} is sufficiently large that the intermediate Krylov vectors cannot be stored and orthogonalized. However, Lanczos diagonalization performs well when it is feasible to orthogonalize the Krylov vectors. Limiting N^{vib} is thus a key issue in this work and as we show below is precisely what the proposed algorithm does.

In the original formulation[2] of the KDC approximation, the normal modes of $\psi_J^{\text{init}}(\mathbf{r}; \mathbf{Q})$ were used to define (initial-state-biased) $|\mathbf{n}(\mathbf{Q})\rangle$. The motivation was to simplify the initial conditions ($d_m^J = \delta_{mJ}$) required to describe short time propagation. However, in the general case, the initial-state-biased basis is poorly positioned to describe the bound vibrational states of the final electronic state. Consequently, N^{vib} must increase significantly to converge $\mathbf{D}^K$. The introduction of final-state-biased bases improves the efficiency of the spectral simulations but sacrifices the convenience of $d_m^J = \delta_{mJ}$. The previously mentioned generating function technique[26] enables convenient evaluation of $\mathbf{d}^J$ at a cost of only $O(N^{\text{vib}}N^{\text{mode}})$, making final-state-biased bases feasible. Several practical final-state-biased bases have been utilized.[26−33]

To determine a vibrational basis, both $|\mathbf{n}(\mathbf{Q})\rangle$ and $\mathbf{N}$ are required as shown in eq 3. The final-state-biased normal modes answer the choice of $|\mathbf{n}(\mathbf{Q})\rangle$, but $\mathbf{N}$ has long been left to chemical intuition plus trial and error. In fact, it is NP-hard to determine $\mathbf{N}$: to find some $\mathbf{N}$ producing a satisfactory spectrum subject to $N^{\text{vib}}(\mathbf{N}) < N_{\text{affordable}}^{\text{vib}}$, where $N_{\text{affordable}}^{\text{vib}}$ is at most one billion with our solver (even smaller if the vibronic wave functions are demanded). Freezing hydrogen stretches while at least singly exciting other modes, a popular rule of thumb, fails when there are 30 or more "other modes", since $N^{\text{vib}} \ge 2^{30} > 10^9$ while still performing poorly. This is the situation encountered in the present work: cyclopentoxide has 39 internal modes, among which only 9 are C−H stretches.

The first step toward an automated $\mathbf{N}$ determination is to define an objective and easy-to-compute quantity as the evaluation standard of a vibrational basis in place of the spectrum itself, which consumes weeks of CPU time and requires a subjective judgment of "satisfaction". There exists a natural criterion for the validity of a final-state-biased basis

$$d(\mathbf{N}) = \sum_{m=1}^{N^{\text{vib}}(\mathbf{N})} |d_m^J|^2 \tag{8}$$

namely, the total overlap between the initial vibrational state and the final-state-biased basis, reflecting how well the initial state can be described. $d(\mathbf{N}) \to 1$ is not only a necessary condition of the basis adequacy but also fairly sufficient for final-state-biased bases. $d(\mathbf{N})$ is a desirable heuristic function in that, first, its value is an unambiguous standard for the basis quality, and second, the cost of evaluating d pales compared to that of diagonalizing $\mathbf{H}$.

As a straightforward idea, one may expect an optimal $\mathbf{N}$ from maximizing $d(\mathbf{N})$ subject to $N^{\text{vib}}(\mathbf{N}) < N_{\text{affordable}}^{\text{vib}}$ and some search algorithm to avoid trying out the myriad of possibilities. Unfortunately, this is an integer inequality constrained nonlinear optimization, whose rigorous solution is too difficult to find. Alternatively, here we propose an inexpensive phenomenological approach based on a continuum model.

Assign an effective length L_i to N_i using standard harmonic oscillator relations

$$L_i^2(N_i) = \langle N_i - 1 | Q_i^2 | N_i - 1 \rangle = \frac{\hbar}{\Omega_i}\left(N_i - \frac{1}{2}\right) \tag{9a}$$

https://dx.doi.org/10.1021/acs.jpclett.0c02199
J. Phys. Chem. Lett. 2020, 11, 7245−7252

$$N_i(L_i) = \frac{\Omega_i}{\hbar} L_i^{\,2} + \frac{1}{2} \tag{9b}$$

where Ω_i is the frequency corresponding to Q_i. Since the multimode vibrational basis function is a direct product of single mode functions, the total effective volume of $\mathbf{N}$ is an N^{mode}-dimensional cuboid centered at the origin of $\mathbf{Q}$. Given that the initial nuclear wave function is usually the ground vibrational level of the initial electronic state, e.g., photoelectron spectra are usually measured from cold anions, the harmonic ground state $\phi^0(\mathbf{Q})$ dominates our consideration. The contour line (isoline) of $\phi^0(\mathbf{Q})$, a product of Gaussian functions, is an ellipsoid centered at the initial state equilibrium geometry and, as one may infer, can be most efficiently covered by a circumscribed cuboid. This covering of the ellipsoid by the cuboid represents the overlap d. Certainly, covering a further isoline produces a larger d. A sketch to visualize this idea in the $N^{\text{mode}} = 2$ case can be found in Figure 1.

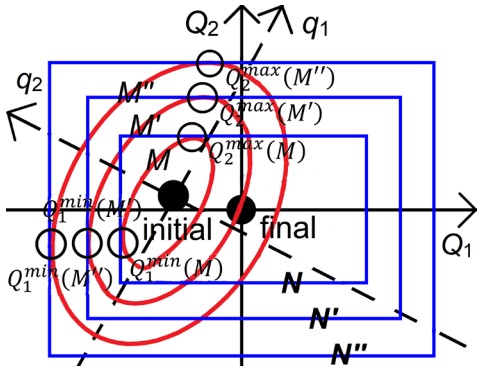

Figure 1. Sketch of the continuum model for the optimal phonon distributions of final-state-biased normal modes in a 2-dimensional case. Scan a batch of initial state contours (red ellipsoids labeled with M, M', M''), use eq 14 to obtain the outermost points along Q_1 and Q_2 (in this case $Q_1^{\min}$ and $Q_2^{\max}$), and determine corresponding distributions by eq 15 (blue cuboids circumscribing the red ellipsoids, labeled with $\mathbf{N}$, $\mathbf{N}'$, $\mathbf{N}''$).

Table 1. Representative Bond Lengths in Å, Bond Angles and Dihedral Angles in Degree, for Cyclopentoxy Radical Ground State Minimum (MIN), $1,2^2$A Minimum Energy Crossing (MEX), and Cyclopentoxide Anion Ground State Minimum (AMIN) from Ref 45

	MIN	MEX	AMIN
C1−O	1.3795	1.3827	1.3321
C1−H1	1.0898	1.0914	1.1171
O−C1−C2	105.4	112.2	112.8
O−C1−C3	111.1	109.8	112.8
H1−C1−C2	111.8	112.6	108.2
H1−C1−C3	113.2	111.6	108.2
C4−C5−C2−C1	−18.1	−18.0	28.8
C3−C4−C5−C2	37.6	37.6	0.0

Mathematically, let $\mathbf{q}$ and $\boldsymbol{\omega}$ be the mass-weighted normal modes and the frequencies of the initial state. Define an M contour

$$M^2 = \sum_{i=1}^{N^{\text{mode}}} \frac{2\omega_i}{\hbar} |q_i|^2 = \mathbf{q}^{\dagger}\Sigma^{-1}q \tag{10}$$

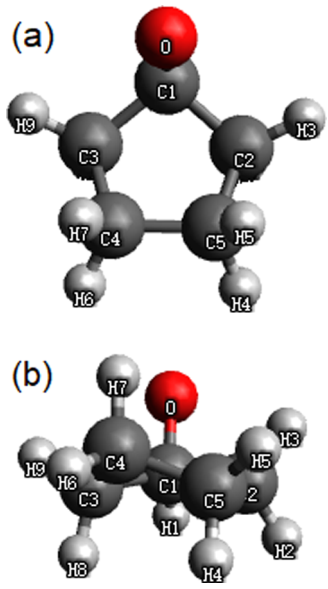

Figure 2. (a) Cyclopentoxide anion and (b) cyclopentoxy radical ground state minima differ mainly in dihedral angles C3−C4−C5−C2 and C4−C5−C2−C1, corresponding to the lowest and the 2nd lowest frequency normal modes. Atom numbering used in text is also indicated.

This is an ellipsoid equation with M adjusting the size of the ellipsoid. As shown in Figure 1, the greater M is, the larger the ellipsoid grows. d is thus proportional to M. The initial and the final states' normal coordinate systems are related by

$$\mathbf{q} = \mathbf{TQ} + \mathbf{b} \tag{11}$$

$\mathbf{T}$ and $\mathbf{b}$ come from the definitions of $\mathbf{q}$ and $\mathbf{Q}$; e.g., if in an arbitrary internal coordinate system the initial (final) state has equilibrium geometry $\mathbf{X}_i$ ($\mathbf{X}_f$) and normal coordinate transformation $\mathbf{L}_i$ ($\mathbf{L}_f$), then

$$\mathbf{q} = \mathbf{L}_i^{-1}(\mathbf{X} - \mathbf{X}_i) \tag{12a}$$

$$\mathbf{Q} = \mathbf{L}_f^{-1}(\mathbf{X} - \mathbf{X}_f) \tag{12b}$$

$$\mathbf{T} = \mathbf{L}_i^{-1}\mathbf{L}_f \tag{12c}$$

$$\mathbf{b} = \mathbf{L}_i^{-1}(\mathbf{X}_f - \mathbf{X}_i) \tag{12d}$$

For a given M, we may map to an $\mathbf{N}(M)$ by finding the circumscribed cuboid of the M contour ellipsoid. To determine that cuboid, along each Q_i direction we must find the outermost point of the ellipsoid, which can be obtained by searching the ellipsoid along each Q_i direction. In the Figure 1 example, the leftmost point $Q_1^{\min}$ and the upmost point $Q_2^{\max}$ are where a cuboid is tangent to an ellipsoid. More formally, this is a minimization (maximization) problem of Q_i, subject to the constraint that the search point must stay on the ellipsoid. Mathematically, this is to minimize (maximize) the merit function

$$f(\mathbf{Q}) = Q_i \tag{13a}$$

subject to the constraint that $\mathbf{Q}$ lies on the ellipsoid

$$c(\mathbf{Q}) \equiv (\mathbf{TQ} + \mathbf{b})^T\Sigma^{-1}(\mathbf{TQ} + \mathbf{b}) - M^2 = 0 \tag{13b}$$

We solve the constrained optimization problem eq 13 by optimizing the augmented Lagrangian[40]

https://dx.doi.org/10.1021/acs.jpclett.0c02199
J. Phys. Chem. Lett. 2020, 11, 7245−7252

Table 2. Phonon Distributions of Representative Final-State-Biased Bases Labeled with M Values[a]

	0.5	0.6	0.7	0.8	0.85	naïve
1	13	13	14	14	14	2
2	26	28	29	30	31	2
3	2	2	2	2	2	2
4	1	1	1	1	1	2
5	1	1	1	1	1	2
6	1	1	1	1	2	2
7	1	1	1	1	2	2
8	1	1	1	1	2	2
9	1	1	1	1	1	2
10	1	1	1	2	2	2
11	1	1	1	2	2	2
12	1	1	1	1	1	2
13	1	1	2	2	2	2
14	1	1	1	1	1	2
15	2	2	2	2	2	2
16	1	1	1	1	1	2
17	1	1	1	1	1	2
18	1	1	1	2	2	2
19	1	1	1	2	2	2
20	1	2	2	2	2	2
21	1	1	1	1	1	2
22	1	1	1	1	1	2
23	1	1	1	2	2	2
24	2	2	2	2	2	2
25	1	1	1	2	2	2
26	3	3	3	3	3	2
27	1	1	1	1	1	2
28	1	1	1	1	1	2
29	1	1	1	1	1	2
30	1	1	1	1	1	2
31	1	1	1	2	2	1
32	1	1	1	1	1	1
33	1	1	1	1	1	1
34	1	1	1	1	2	1
35	1	1	1	1	2	1
36	1	1	1	1	1	1
37	1	1	1	1	1	1
38	1	1	1	1	1	1
39	1	1	1	1	1	1
N^{vib}	8112	17 472	38 976	5 160 960	170 655 744	1 073 741 824
d	0.814 89	0.837 507	0.856 825	0.910 176	0.930 219	~0

[a]The basis origin is cyclopentoxy radical 1,2^{2}A minimum energy crossing. "Naïve" denotes "2 phonons per mode except the C−H stretches" rather than an optimal distribution.

$$L(\mathbf{Q}) = f(\mathbf{Q}) - \lambda c(\mathbf{Q}) + \mu c^2(\mathbf{Q}) \tag{14}$$

where λ and μ are the augmented Lagrange multipliers. The initial values in our implementation are $\lambda = 0$ and $\mu = 0.5$. Once the minimizer $Q_i^{\min}(M)$ and the maximizer $Q_i^{\max}(M)$ are determined, eq 9b gives $N_i(M)$ as

$$N_i(M) = \left\lceil \frac{\Omega_i}{\hbar} \max^2(|Q_i^{\min}(M)|, |Q_i^{\max}(M)|) + \frac{1}{2} \right\rceil \tag{15}$$

where $\lceil x \rceil$ takes the smallest integer no less than x. Thus, the minimum value of N_i is 1, which is consistent with eq 9. The $d(\mathbf{N})$ optimization problem is thus reduced to a simple univariate one, namely, searching for the largest M subject to $N^{vib}[\mathbf{N}(M)] < N^{vib}_{affordable}$. By analogy to 1-dimensional Gaussians, where 2-sigma covers 95%, a satisfactory $d[\mathbf{N}(M)]$ should arise before M reaches 2, so M lies within a narrow range $(0, 2)$.

It is worthwhile to note that the $d[\mathbf{N}(M)]$ optimization can be reinterpreted: one can conveniently tune a final-state-biased basis by manipulating M, systematically approaching the complete basis limit in an optimal way. For example, one can diagonalize eq 6 using a small $\mathbf{N}(M)$ to simulate the entire spectrum and obtain all important eigenstates and then repeat the calculation using a large $\mathbf{N}(M)$ focusing on the low levels to establish convergence of the small $\mathbf{N}(M)$ result. This approach can be used, for example, to include geometry-dependent spin−orbit coupling in a calculation.

We apply our algorithm to cyclopentoxide anion ($C_5H_9O^-$) photoelectron detachment to further illustrate our method. Figure 2 pictures $C_5H_9O^-$ and the electron-detached species (cyclopentoxy radical, C_5H_9O) equilibrium geometries and indicates the atom labeling. Table 1 provides the values of key internal coordinates. $C_5H_9O^-$ has C_s point group symmetry

https://dx.doi.org/10.1021/acs.jpclett.0c02199
J. Phys. Chem. Lett. 2020, 11, 7245−7252

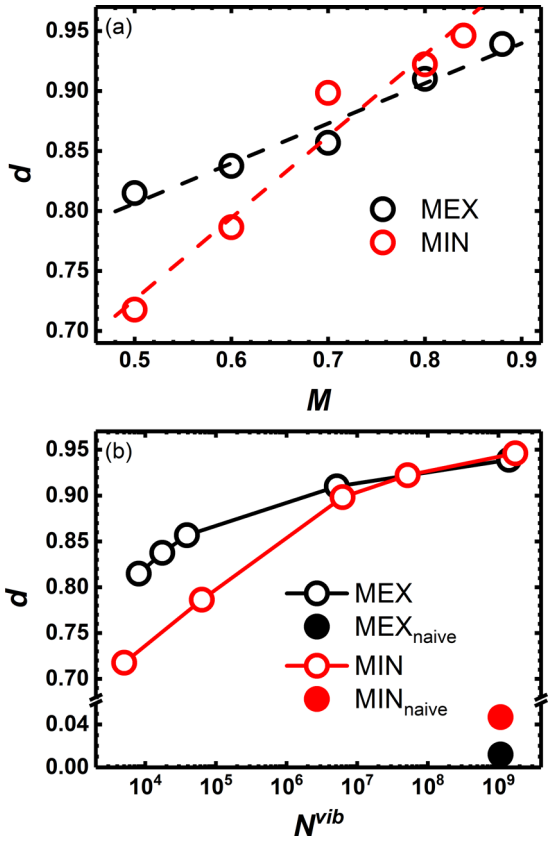

Figure 3. d values of final-state-biased bases as a function of (a) M and (b) vibrational basis size N^{vib}. Two series of bases are positioned at cyclopentoxy radical $1,2^2A$ minimum energy crossing (MEX) and ground state minimum (MIN), respectively. "Naïve" denotes "2 phonons per mode except the C−H stretches" rather than an optimal distribution.

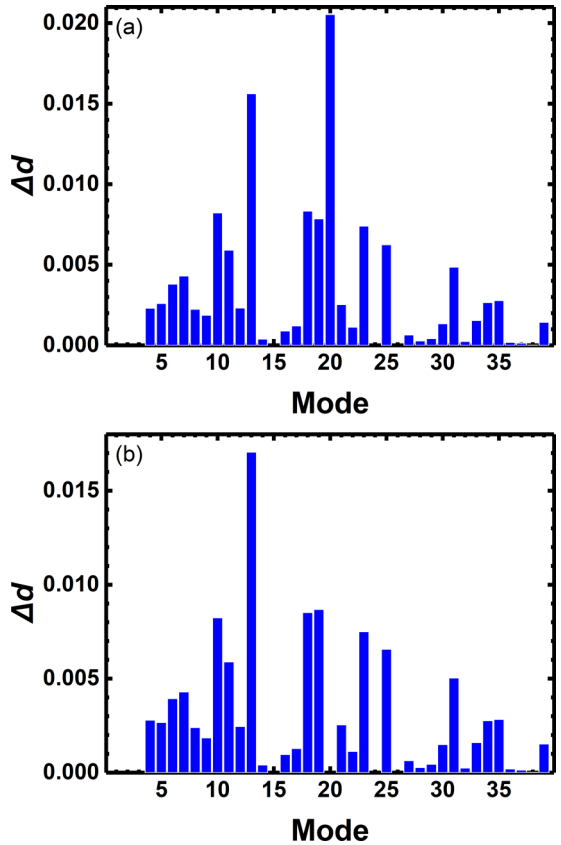

Figure 4. Based on the (a) $M = 0.5$ and (b) 0.6 bases (2nd and 3rd columns in Table 1), adding a phonon to a mode i (N_i: 1 → 2) raises d by Δd. Activation of mode (a) 20 and (b) 13 produces the most gain.

while C_5H_9O has C_1 symmetry. This symmetry breaking corresponds to huge 40° distortions in dihedral angles C3−C4−C5−C2 and C4−C5−C2−C1. The two lowest states of C_5H_9O have a low-lying conical intersection producing a Jahn−Teller type interaction[41] that couples the corresponding potential energy surfaces.

The C_5H_9O conical intersection necessitates the use of a 2-state quasidiabatic Hamiltonian ($\mathbf{H}^d$) to describe the electronic structure. $\mathbf{H}^d$ was constructed in a previous work[42] using multireference configuration interaction with single and double excitations (MRCISD) wave functions based on 6 frozen core orbitals, 15 doubly occupied orbitals, and a 5-electron 3-orbital active space. An atomic orbital basis set which is cc-pVTZ[43] for the oxygen and the carbons and cc-pVDZ[43] for the hydrogens was used. The MRCISD expansion is composed of 19 302 445 configuration state functions (CSFs). For the closed-shell anion $C_5H_9O^-$ the above-described MRCISD was replaced by a single reference CISD expansion with 6 frozen core orbitals and 18 doubly occupied orbitals, with the atomic orbital basis set for oxygen extended to aug-cc-pVTZ.[44] The CISD expansion is composed of 7 634 278 CSFs. All electronic structure data used in this work were reported previously[45] and employed the COLUMBUS[46−54] suite of programs. The MRCISD evinces a $1,2^2A$ minimum energy crossing (MEX) structure for C_5H_9O that deviates slightly from its ground state minimum (MIN) and is only 0.064 eV higher in energy (see Table 1). The adiabatic electron affinity calculated by the MRCISD and the CISD electronic energies and harmonic frequencies is 1.2 eV.

The experimental spectrum[55] is measured from cryogenic $C_5H_9O^-$ photoionized at 532 nm (and 355 nm, omitted due to no new feature). The independence of photoionization to wavelength validates the Franck−Condon approximation. The broad peak observed in experiment supports a large geometry difference between $C_5H_9O^-$ and C_5H_9O. The measured adiabatic electron affinity is 1.5 eV.

The huge 40° distortions in dihedral angles C3−C4−C5−C2 and C4−C5−C2−C1 increase the difficulty in using the KDC approximation to describe vibronic coupling. First, it is hopeless to manually determine the phonon distribution. In a previous work on propyne,[33] the overlap between the harmonic vibrational ground states of the neutral and the cation is already 0.7, while that of $C_5H_9O^-$ plunges to 0.000 024 (recall from eq 8 that $d \to 1$ is a necessary condition of the basis adequacy). As a consequence, for propyne it is tolerable to determine the phonon distribution by trial and error, while that becomes hopeless for $C_5H_9O^-$. Second, many phonons must be placed in the normal modes corresponding to C3−C4−C5−C2 and C4−C5−C2−C1, leading to large vibronic Hamiltonian matrix elements, deteriorating the fragile numerical stability of the Lanczos algorithm. This is the case encountered in this work: Even for the smallest basis tested ($N^{vib} \sim 10^4$), the zero-point energy can be in error by 7 eV without orthogonalizing the Krylov vectors. This orthogonalization is feasible only with the compact basis, since there are additional $O(N^{vib}N^{iter})$ storage and $O(N^{vib}[N^{iter}]^2)$ computational requirements in the orthogonalized Lanczos diagonalization, where N^{iter} is the

https://dx.doi.org/10.1021/acs.jpclett.0c02199
J. Phys. Chem. Lett. 2020, 11, 7245−7252

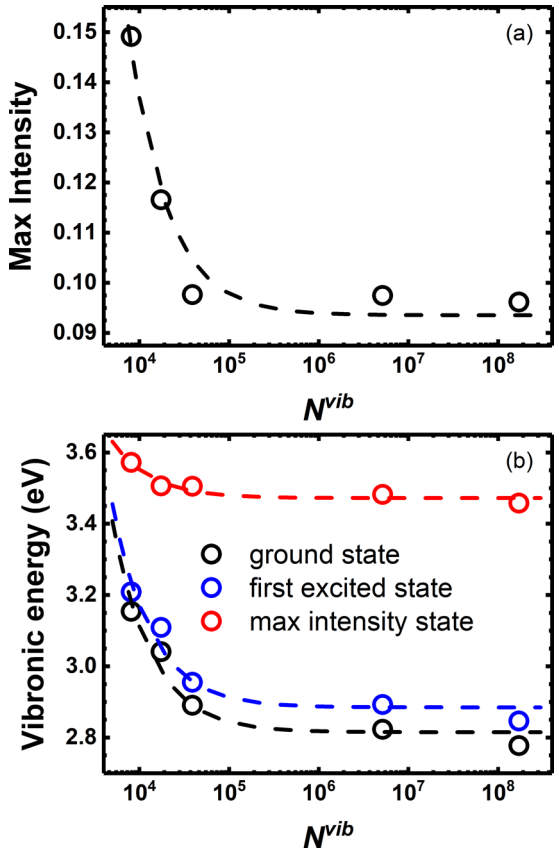

Figure 5. (a) Intensity of the max intensity line as a function of vibrational basis size N^{vib}. (b) Energies of cyclopentoxy radical vibronic ground state, 1st excited state, and max intensity state. The zero of energy is taken as that of cyclopentoxy radical ground state minimum.

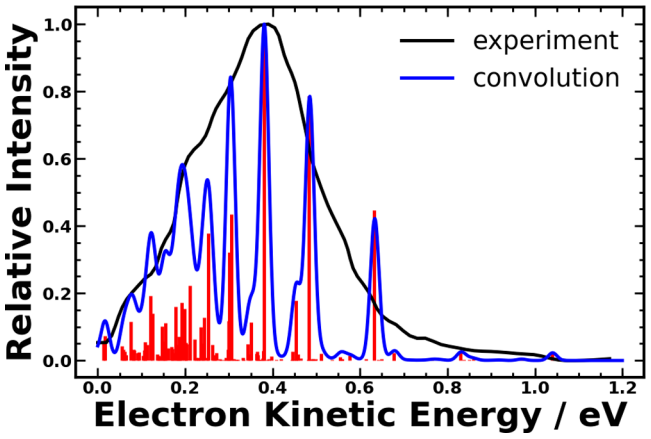

Figure 6. Simulated photoelectron spectrum of cyclopentoxide anion, in comparison to the supersonic expansion cryogenic experiment from ref 55. A Gaussian function with 0.01 eV width is adopted for convolution.

number of iterations. Given our resources (1 TB hard disk and 24 CPUs), $N^{vib} < 10^7$ is the most we can afford to simulate the entire spectrum and obtain all important eigenstates.

Figure 3 demonstrates two series of final-state-biased bases positioned at C_5H_9O MEX and MIN. The normal modes are defined by diagonalizing $\nabla\nabla\left(\frac{H_{11}^d + H_{22}^d}{2}\right)$ and the adiabatic ground state Hessian, respectively. Figure 3a shows that $d \propto M$, as expected by our continuum model: the covering of the ellipsoid by the cuboid is equivalent to the overlap d, and covering a larger isoline (M) produces a greater d. The dash lines are the linear regressions, whose coefficients of determination are both 96%, and extrapolations predict that for MEX (MIN) $d \rightarrow 1$ will be reached when $M \rightarrow 1.08$ (0.90). Exact d values cannot be computed for such M due to the overwhelming N^{vib}. Figure 3b shows that, despite the large molecular size, the optimal phonon distribution can give small but adequate bases. The details of phonon distributions for the MEX bases can be found in Table 2. The performance of the smallest naïve distribution (2 phonons per mode except the C−H stretches) is also reported Figure 3b. Although its size exceeds one billion, the resulting d value is less than 0.05. On the contrary, our optimized distributions routinely give $d > 0.7 \gg 0.05$ requiring only $N^{vib} \sim 10^4$.

From Figure 4 and Table 2 we illustrate that our continuum model always finds the optimum mode(s) to improve an existing $d[\mathbf{N}(M)]$. From Table 2, we see that the largest change from $M = 0.5$ to 0.6 (M: 0.5 → 0.6) is the activation of the single, previously frozen, mode 20 (N_{20}: 1 → 2). Similarly the result for M: 0.6 → 0.7 is N_{13}: 1 → 2. Figure 4a,b, respectively, shows that, not surprisingly, placing a phonon in mode 20 (13) produces the largest increase in d on any single replacement as our continuum model predicts. In the general case, when more than one mode is excited manual trial and error selection of groups of modes is no longer feasible, but one can always rely on our continuum model.

We demonstrate the fast convergence of our final-state-biased bases in Figure 5. The MEX basis is chosen since it is found in Figure 3 to perform better when N^{vib} is small. Figure 5a reports the N^{vib} dependence of the intensity of the maximum intensity line (MIL). This figure shows that the MIL converges as a function of N^{vib}. Particularly gratifying is the small change in the MIL with large change in N^{vib} for N^{vib} large. Similar convergent behavior is reported in Figure 5b for the energies of the ground state (the zero-point energy), the first excited state, and the MIL.

These observations are quantified by the fits to the intensity and the energies provided by the dashed lines in Figure 5. A complete basis set limit extrapolation of any observable O is given by

$$O(N^{vib}) = \frac{a}{N^{vib}} + O_\infty \tag{16}$$

where a and O_∞ are extrapolation parameters. From the analyses $N^{vib} = 38\,976$ ($M = 0.7$, $d = 86\%$) is seen to well converge the MIL, while the low-lying states require $N^{vib} = 5\,160\,960$ ($M = 0.8$, $d = 91\%$) to converge reasonably. The faster convergence of the MIL is as anticipated, since our continuum model is designed to bias the MIL.

Given $N^{vib} = 5\,160\,960$ ($M = 0.8$, $d = 91\%$) has proven to be converged in Figure 5, we simulate the photoelectron spectrum with this basis, and the result is presented in Figure 6. A Gaussian function with 0.01 eV width is adopted for convolution. For comparison, the simulated and measured intensity maxima are made to agree, accounting principally for the difference in the calculated and the measured adiabatic electron affinities. The simulation well reproduces the experiment: the peak heights match the experiment between 0.3 and 1.2 eV; the convolution overlays the experiment between 0 and 0.2 eV. The convolution is not as broad as the experiment between 0.2 and 1.2 eV.

To sum up, we have reported a continuum model enabling automatic generation of compact multimode vibrational bases for spectral simulations of moderate-sized molecules. The

https://dx.doi.org/10.1021/acs.jpclett.0c02199
J. Phys. Chem. Lett. 2020, 11, 7245−7252

photoelectron spectrum of cyclopentoxide has been determined using this algorithm and compared with experiment. The compact representation can be adapted to incorporate the geometry-dependent spin−orbit interaction into the non-relativistic eigenstate representation. In the future these tools will be applied to analyze fine-structure quenching in cyclopentoxy vibronic wave functions.

AUTHOR INFORMATION

Corresponding Authors

Yifan Shen − *Department of Chemistry, Johns Hopkins University, Baltimore, Maryland 21218, United States;* orcid.org/0000-0003-0590-444X; Email: yifanshensz@jhu.edu

David R. Yarkony − *Department of Chemistry, Johns Hopkins University, Baltimore, Maryland 21218, United States;* orcid.org/0000-0002-5446-1350; Email: yarkony@jhu.edu

Complete contact information is available at: https://pubs.acs.org/10.1021/acs.jpclett.0c02199

Notes

The authors declare no competing financial interest.

ACKNOWLEDGMENTS

This work was supported by National Science Foundation grant (CHE-1663692) to D.R.Y. The authors are grateful for a grant of computer time on the Maryland Advanced Research Computing Center (MARCC) at Johns Hopkins University. The authors are grateful to Professor Lan Cheng (Johns Hopkins University) for sharing hard disk and Professor Robert Continetti (University of California, San Diego) for helpful discussion on the details of his experiment.

REFERENCES

(1) Köppel, H.; Domcke, W.; Cederbaum, L. S. *Conical Intersections*; Domcke, W., Yarkony, D. R., Eds.; World Scientific: NJ, 2004.

(2) Köuppel, H.; Domcke, W.; Cederbaum, L. S. Multimode Molecular Dynamics Beyond the Born-Oppenheimer Approximation. *Adv. Chem. Phys.* **1984**, *57*, 59−246.

(3) Pacher, T.; Cederbaum, L. S.; Köppel, H. Adiabatic and Quasidiabatic States in a Gauge Theoretical Framework. *Adv. Chem. Phys.* **2007**, *84*, 293.

(4) Köppel, H.; Döscher, M.; Bâldea, I.; Meyer, H.-D.; Szalay, P. G. Multistate Vibronic Interactions in the Benzene Radical Cation. II. Quantum Dynamical Simulations. *J. Chem. Phys.* **2002**, *117*, 2657−2671.

(5) Stanton, J. F.; Sattelmeyer, K. W.; Gauss, J.; Allan, M.; Skalicky, T.; Bally, T. On the Photoelectron Spectrum of p-Benzoquinone. *J. Chem. Phys.* **2001**, *115*, 1−4.

(6) Nooijen, M. First-Principles Simulation of the UV Absorption Spectrum of Ketene. *Int. J. Quantum Chem.* **2003**, *95*, 768−783.

(7) Hazra, A.; Nooijen, M. Vibronic Coupling in the Excited Cationic States of Ethylene: Simulation of the Photoelectron Spectrum between 12 and 18eV. *J. Chem. Phys.* **2005**, *122*, 204327.

(8) Hazra, A.; Nooijen, M. Comparison of Various Franck−Condon and Vibronic Coupling Approaches for Simulating Electronic Spectra: The Case of the Lowest Photoelectron Band of Ethylene. *Phys. Chem. Chem. Phys.* **2005**, *7*, 1759−1771.

(9) Motzke, A.; Lan, Z.; Woywod, C.; Domcke, W. Simulation of the Photodetachment Spectrum of the Pyrrolide Anion. *Chem. Phys.* **2006**, *329*, 50−64.

(10) Ichino, T.; Gianola, A. J.; Lineberger, W. C.; Stanton, J. F. Nonadiabatic Effects in the Photoelectron Spectrum of the Pyrazolide-d_3 Anion: Three-State Interactions in the Pyrazolyl- d_3 Radical. *J. Chem. Phys.* **2006**, *125*, 084312.

(11) Ichino, T.; Wren, S. W.; Vogelhuber, K. M.; Gianola, A. J.; Lineberger, W. C.; Stanton, J. F. The Vibronic Level Structure of the Cyclopentadienyl Radical. *J. Chem. Phys.* **2008**, *129*, 084310.

(12) Stanton, J. F. On the Vibronic Level Structure in the NO_3 Radical. I. The Ground Electronic State. *J. Chem. Phys.* **2007**, *126*, 134309.

(13) Stanton, J. F. On the Vibronic Level Structure in the NO_3 Radical: II. Adiabatic Calculation of the Infrared Spectrum. *Mol. Phys.* **2009**, *107*, 1059−1075.

(14) Stanton, J. F.; Okumura, M. On the Vibronic Level Structure in the NO_3 Radical : Part III. Observation of Intensity Borrowing via Ground State Mixing. *Phys. Chem. Chem. Phys.* **2009**, *11*, 4742.

(15) Weichman, M. L.; Cheng, L.; Kim, J. B.; Stanton, J. F.; Neumark, D. M. Low-Lying Vibronic Level Structure of the Ground State of the Methoxy Radical: Slow Electron Velocity-Map Imaging (SEVI) Spectra and Köppel-Domcke-Cederbaum (KDC) Vibronic Hamiltonian Calculations. *J. Chem. Phys.* **2017**, *146*, 224309.

(16) Rabidoux, S. M.; Cave, R. J.; Stanton, J. F. Nonadiabatic Investigation of the Electronic Spectroscopy of *trans*-1,3-Butadiene. *J. Phys. Chem. A* **2019**, *123*, 3255−3271.

(17) Schuurman, M. S.; Young, R. A.; Yarkony, D. R. On the Multimode Quadratic Vibronic Coupling Problem: An Open-Ended Solution Using a Parallel Lanczos Algorithm. *Chem. Phys.* **2008**, *347*, 57−64.

(18) Light, J. C.; Hamilton, I. P.; Lill, J. V. Generalized Discrete Variable Approximation in Quantum Mechanics. *J. Chem. Phys.* **1985**, *82*, 1400−1409.

(19) Bowman, J. M.; Carrington, T.; Meyer, H.-D. Variational Quantum Approaches for Computing Vibrational Energies of Polyatomic Molecules. *Mol. Phys.* **2008**, *106*, 2145−2182.

(20) Carter, S.; Handy, N. C. A Variational Method for the Calculation of Vibrational Levels of Any Triatomic Molecule. *Mol. Phys.* **1982**, *47*, 1445−1455.

(21) Carter, S.; Handy, N. C. The Variational Method for the Calculation of RO-Vibrational Energy Levels. *Comput. Phys. Rep.* **1986**, *5*, 117−171.

(22) Celani, P.; Bernardi, F.; Olivucci, M.; Robb, M. A. Conical Intersection Mechanism for Photochemical Ring Opening in Benzospiropyran Compounds. *J. Am. Chem. Soc.* **1997**, *119*, 10815−10820.

(23) Migani, A.; Robb, M. A.; Olivucci, M. Relationship between Photoisomerization Path and Intersection Space in a Retinal Chromophore Model. *J. Am. Chem. Soc.* **2003**, *125*, 2804−2808.

(24) Yarkony, D. R. Nonadiabatic Quantum Chemistry—Past, Present, and Future. *Chem. Rev.* **2012**, *112*, 481−498.

(25) Domcke, W.; Yarkony, D. R. Role of Conical Intersections in Molecular Spectroscopy and Photoinduced Chemical Dynamics. *Annu. Rev. Phys. Chem.* **2012**, *63*, 325−352.

(26) Schuurman, M. S.; Yarkony, D. R. A Method to Reduce the Size of the Vibronic Basis Employed in the Simulation of Spectra Using the Multimode Vibronic Coupling Approximation. *J. Chem. Phys.* **2008**, *128*, 044119.

(27) Schuurman, M. S.; Yarkony, D. R. A Simulation of the Photoelectron Spectrum of Pyrazolide. *J. Chem. Phys.* **2008**, *129*, 064304.

(28) Papas, B. N.; Schuurman, M. S.; Yarkony, D. R. The Simulated Photoelectron Spectrum of 1-Propynide. *J. Chem. Phys.* **2009**, *130*, 064306.

(29) Dillon, J. J.; Yarkony, D. R. The Photoelectron Spectrum of the Ethoxide Anion: Conical Intersections, the Spin-Orbit Interaction, and Sequence Bands. *J. Chem. Phys.* **2009**, *131*, 134303.

(30) Dillon, J. J.; Yarkony, D. R. The Photoelectron Spectrum of the Isopropoxide Anion: Nonadiabatic Effects Due to Conical Intersections and the Spin-Orbit Interaction. *J. Chem. Phys.* **2009**, *130*, 154312.

(31) Zhu, X.; Yarkony, D. R. The Photoelectron Spectrum of Pyrrolide: Nonadiabatic Effects Due to Conical Intersections. *J. Phys. Chem. C* **2010**, *114*, 5312−5320.

(32) Dillon, J.; Yarkony, D. R. Nonadiabatic Effects in Substitutional Isomers of Jahn-Teller Molecules: The Strange Case of Hydroxymethoxy. *J. Chem. Phys.* **2012**, *137*, 154315.
(33) Marquez, S.; Dillon, J.; Yarkony, D. R. On the Photoionization Spectrum of Propyne: A Fully Ab Initio Simulation of the Low-Energy Spectrum Including the Jahn−Teller Effect and the Spin−Orbit Interaction. *J. Phys. Chem. A* **2013**, *117*, 12002−12010.
(34) Baer, M. Adiabatic and Diabatic Representations for Atom-Molecule Collisions: Treatment of the Collinear Arrangement. *Chem. Phys. Lett.* **1975**, *35*, 112−118.
(35) Mead, C. A.; Truhlar, D. G. Conditions for the Definition of a Strictly Diabatic Electronic Basis for Molecular Systems. *J. Chem. Phys.* **1982**, *77*, 6090−6098.
(36) Han, S.; Yarkony, D. R. On the Determination of Intensities for Electron Photodetachment and Photoionization Spectra Involving States Coupled by Conical Intersections: Total Integral Cross Sections for Polyatomic Molecules. *J. Chem. Phys.* **2010**, *133*, 194107.
(37) Han, S.; Yarkony, D. R. Determining Partial Differential Cross Sections for Low-Energy Electron Photodetachment Involving Conical Intersections Using the Solution of a Lippmann-Schwinger Equation Constructed with Standard Electronic Structure Techniques. *J. Chem. Phys.* **2011**, *134*, 174104.
(38) Han, S.; Yarkony, D. R. On the Determination of Partial Differential Cross Sections for Photodetachment and Photoionization Processes Producing Polyatomic Molecules with Electronic States Coupled by Conical Intersections. *J. Chem. Phys.* **2011**, *134*, 134110.
(39) Han, S.; Yarkony, D. R. A Lippmann−Schwinger Approach for the Determination of Photoionization and Photodetachment Cross Sections Based on a Partial Wave Green's Function Expansion and Configuration Interaction Wave Functions. *Mol. Phys.* **2012**, *110*, 845−859.
(40) Nocedal, J.; Wright, S. J. *Numerical Optimization*, 2nd ed.; Mikosch, T. V., Resnick, S. I., Robinson, S. M., Eds.; Springer: New York, 2006.
(41) Barckholtz, T. A.; Miller, T. A. Quantitative Insights about Molecules Exhibiting Jahn-Teller and Related Effects. *Int. Rev. Phys. Chem.* **1998**, *17*, 435−524.
(42) Shen, Y.; Yarkony, D. R. Construction of Quasi-Diabatic Hamiltonians That Accurately Represent Ab Initio Determined Adiabatic Electronic States Coupled by Conical Intersections for Systems on the Order of 15 Atoms. Application to Cyclopentoxide Photoelectron Detachment in the Full 39 Degrees of Freedom. *J. Phys. Chem. A* **2020**, *124*, 4539−4548.
(43) Dunning, T. H. Gaussian Basis Sets for Use in Correlated Molecular Calculations. I. The Atoms Boron through Neon and Hydrogen. *J. Chem. Phys.* **1989**, *90*, 1007−1023.
(44) Kendall, R. A.; Dunning, T. H.; Harrison, R. J. Electron Affinities of the First-row Atoms Revisited. Systematic Basis Sets and Wave Functions. *J. Chem. Phys.* **1992**, *96*, 6796−6806.
(45) Malbon, C. L.; Yarkony, D. R.; Zhu, X. On the Electronic Structure of the Ground State of Cyclopentoxy. The Case for a Two Coupled State Description. *J. Mol. Spectrosc.* **2015**, *311*, 36−41.
(46) Lischka, H.; Müller, T.; Szalay, P. G.; Shavitt, I.; Pitzer, R. M.; Shepard, R. Columbus—a Program System for Advanced Multireference Theory Calculations. *Wiley Interdiscip. Rev.: Comput. Mol. Sci.* **2011**, *1*, 191−199.
(47) Shepard, R. Geometrical Energy Derivative Evaluation with MRCI Wave Functions. *Int. J. Quantum Chem.* **1987**, *31*, 33−44.
(48) Shepard, R. *Modern Electronic Structure Theory Part I*; Yarkony, D. R., Ed.; World Scientific: Singapore, 1995.
(49) Lischka, H.; Shepard, R.; Pitzer, R. M.; Shavitt, I.; Dallos, M.; Müller, T.; Szalay, P. G.; Seth, M.; Kedziora, G. S.; Yabushita, S.; et al. High-Level Multireference Methods in the Quantum-Chemistry Program System COLUMBUS: Analytic MR-CISD and MR-AQCC Gradients and MR-AQCC-LRT for Excited States, GUGA Spin−Orbit CI and Parallel CI Density. *Phys. Chem. Chem. Phys.* **2001**, *3*, 664−673.
(50) Lischka, H.; Shepard, R.; Shavitt, I.; Pitzer, R. M.; Dallos, M.; Müller, T.; Szalay, P. G.; Brown, F. B.; Ahlrichs, R.; Böhm, H. J. *COLUMBUS, an Ab Initio Electronic Structure Program*, release 7.0; 2017.
(51) Lischka, H.; Dallos, M.; Shepard, R. Analytic MRCI Gradient for Excited States: Formalism and Application to the n-Π* Valence- and n-(3s,3p) Rydberg States of Formaldehyde. *Mol. Phys.* **2002**, *100*, 1647−1658.
(52) Shepard, R.; Lischka, H.; Szalay, P. G.; Kovar, T.; Ernzerhof, M. A General Multireference Configuration Interaction Gradient Program. *J. Chem. Phys.* **1992**, *96*, 2085−2098.
(53) Lischka, H.; Dallos, M.; Szalay, P. G.; Yarkony, D. R.; Shepard, R. Analytic Evaluation of Nonadiabatic Coupling Terms at the MR-CI Level. I. Formalism. *J. Chem. Phys.* **2004**, *120*, 7322−7329.
(54) Dallos, M.; Lischka, H.; Shepard, R.; Yarkony, D. R.; Szalay, P. G. Analytic Evaluation of Nonadiabatic Coupling Terms at the MR-CI Level. II. Minima on the Crossing Seam: Formaldehyde and the Photodimerization of Ethylene. *J. Chem. Phys.* **2004**, *120*, 7330−7339.
(55) Alconcel, L. S.; Continetti, R. E. Dissociation Dynamics and Stability of Cyclopentoxy and Cyclopentoxide. *Chem. Phys. Lett.* **2002**, *366*, 642−649.

https://dx.doi.org/10.1021/acs.jpclett.0c02199
J. Phys. Chem. Lett. 2020, 11, 7245−7252